

A contactless method for measuring the recombination velocity of an individual grain boundary in thin-film photovoltaics

B. G. Mendis,^{a)} L. Bowen, and Q. Z. Jiang

Department of Physics, Durham University, South Road, Durham DH1 3LE, United Kingdom

(Received 22 June 2010; accepted 17 August 2010; published online 2 September 2010)

A cathodoluminescence-based, contactless method for extracting the bulk minority carrier diffusion length and reduced recombination velocity of an individual grain boundary is applied to vapor grown CdTe epitaxial films. The measured diffusion length was within the range of 0.4–0.6 μm and the grain boundary recombination velocity varied from 500 to 750 cm/s. The technique can be used to investigate the effect of grain boundaries on photovoltaic performance. © 2010 American Institute of Physics. [doi:10.1063/1.3486482]

Thin-film photovoltaics, such as those based on CdTe and Cu(In,Ga)Se₂, are viable alternatives to Si-based solar cells due to the small volume of absorber material required and relatively cheap mass production routes.^{1–3} The thin-films have a grain size of only a few micrometer, so that grain boundaries limit charge collection, and hence overall efficiency, of the solar cell. Indeed in CdTe solar cells a CdCl₂ activation step, which passivates the grain boundaries, is used to improve the efficiency by nearly an order of magnitude.^{2,3} It is therefore important to understand how an individual grain boundary affects photovoltaic performance, and characterize its dependence on doping level and illumination intensity, two parameters that affect the grain boundary barrier height.^{4,5}

At the grain boundary region elastic strain fields, dangling bonds and any segregated atoms give rise to electronic states within the band gap which, depending on the relative capture cross-sections for electrons and holes, can act as trap or recombination sites. At steady state the enhanced recombination rate at a grain boundary is balanced by a diffusive flux of carriers toward the boundary from the bulk. The magnitude of the flux is determined by the recombination velocity, which is inversely related to the minority carrier lifetime. A large recombination velocity therefore implies a short lifetime and reduced collection efficiency.

The high energy electrons in a scanning electron microscope (SEM) create electron-hole pairs that, during relaxation, give rise to cathodoluminescence (CL).^{6,7} For low beam currents the CL intensity is in general proportional to the number of excess carriers at steady state. A lower CL intensity is therefore expected for a probe incident close to a grain boundary, due to loss of some of the carriers to the grain boundary diffusion current. van Roosbroeck⁸ has derived the steady state carrier density distribution normal to a free surface, in a semi-infinite solid that does not contain any other free surfaces. Carrier generation is assumed to take place uniformly in a plane parallel to the free surface and is time-independent. The generation plane is at a distance x_b from the free surface which is arbitrarily assigned the position $x=0$. By replacing the free surface in the van Roosbroeck model with a grain boundary, the CL intensity [$I(x_b)$] for

an electron probe incident at distance x_b from the grain boundary is given by the following:

$$I(x_b) = k \int_0^{\infty} \eta(x) \left[\exp\left(-\frac{|x-x_b|}{L}\right) - \frac{S-1}{S+1} \exp\left\{-\frac{(x+x_b)}{L}\right\} \right] dx, \quad (1)$$

where L is the minority carrier diffusion length in the perfect crystal and S is the reduced recombination velocity (i.e., $S = s\tau/L$, where s is the recombination velocity and τ the minority carrier lifetime in the perfect crystal). The terms within the square brackets is the steady state carrier density at the position x (Ref. 8) and the “|” symbol in the first exponential denotes the absolute value. The number of carriers diffusing past the grain boundary is assumed to be negligible, and hence the integration is from zero to infinity (i.e., only on that side of the grain boundary in which the electron beam is incident). The constant k accounts for CL measurement artifacts such as absorption and total internal reflection of the photons as well as detector quantum efficiency.⁶ The radiative recombination efficiency η is the fraction of recombination events leading to photon emission. If η is assumed to be independent of position x (this assumption will be discussed later on) Eq. (1) simplifies as follows:

$$\ln[\Delta I(x_b)] = \ln \left[1 - \frac{I(x_b)}{I(x_b = \infty)} \right] = \ln \left(\frac{S}{S+1} \right) - \frac{x_b}{L}, \quad (2)$$

$I(x_b = \infty)$ is effectively the CL intensity for the perfect crystal. A plot of $\ln[\Delta I(x_b)]$ versus x_b is a straight line, and L and S can be extracted from the gradient and intercept, respectively. If the minority carrier lifetime τ is known the recombination velocity s can be calculated from values of L and S . CL is a contactless technique and by utilizing the high spatial resolution of an SEM the recombination velocity of a single grain boundary can be measured. Furthermore, complementary SEM techniques such as energy/wavelength dispersive x-ray and electron backscattered diffraction can be used to relate the recombination velocity of a grain boundary to its composition and misorientation. Donolato⁹ proposed using the area and variance of the electron beam induced current (EBIC) profile across a grain boundary to determine the minority carrier diffusion length and recombination velocity. However, the EBIC method is restricted to grain boundaries

^{a)}Electronic mail: b.g.mendis@durham.ac.uk.

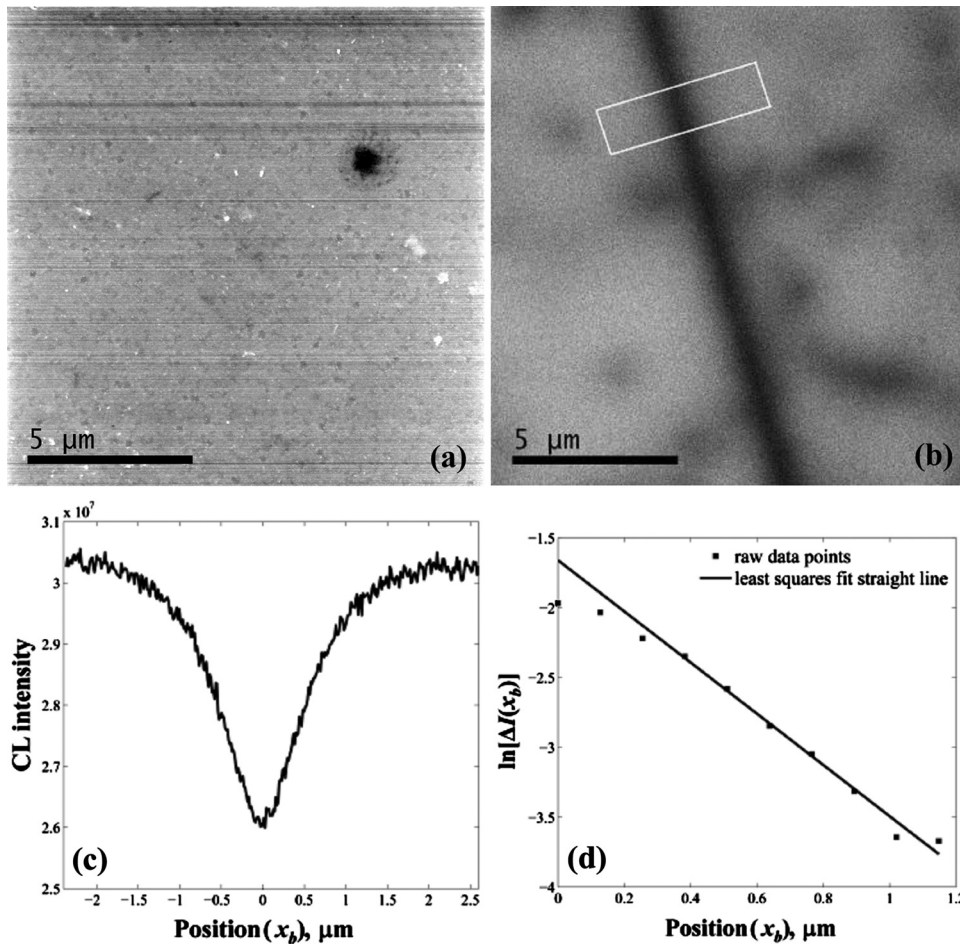


FIG. 1. SE (a) and panchromatic CL (b) images of a CdTe grain boundary. The CL intensity profile normal to the grain boundary, extracted from the box region in (b), is shown in (c); the grain boundary is at the zero position. (d) shows the corresponding $\ln[\Delta I(x_b)]$ vs x_b plot.

perpendicular to the p-n junction and requires a suitable model for the depth generation of carriers before the parameters of interest can be extracted.

In this study, reduced grain boundary recombination velocities are measured in a $\sim 70 \mu\text{m}$ thick, p-type CdTe film epitaxially grown on a Ge substrate using closed space sublimation¹⁰ and subsequently chemically polished in a bromine-methanol solution. Vapor grown CdTe is known to contain subgrain boundaries.¹¹ The sample was examined in a Hitachi SU-70 SEM operating at 15 kV with a Gatan MonoCL system. The electron beam current was $\sim 1.5 \text{ nA}$ and in the regime where the CL intensity is directly proportional to the probe current. Monte Carlo simulation of the electron beam generation volume was carried out assuming screened Rutherford cross-sections and continuous energy loss (for more details see Refs. 6 and 12).

Figures 1(a) and 1(b) show the secondary electron (SE) and panchromatic CL images of a CdTe grain boundary. Only long, straight grain boundaries with narrow width were selected for analysis, so that the boundary is likely to be end-on. No grain boundary grooving is seen in the SE image, so that CL emission is not affected by any change in the electron backscattering coefficient and/or change in the total internal reflection of photons. The integrated CL intensity profile in a direction normal to the grain boundary was extracted from the box region in Fig. 1(b) and is shown in Fig. 1(c). The CL linetrace is used to plot $\ln[\Delta I(x_b)]$ versus x_b as shown in Fig. 1(d). The data points for large x_b generally satisfy a linear relationship although deviations from linearity are observed closer to the grain boundary. In Eq. (2) it

was assumed that η is independent of position. η is given by $\tau_{\text{nr}}/(\tau_{\text{nr}} + \tau_{\text{r}})$, where τ_{nr} and τ_{r} are the nonradiative and radiative lifetimes, respectively. Deep states at a grain boundary are typically nonradiative recombination centers, and hence decrease τ_{nr} and η . This means less efficient CL emission for a given carrier density at the grain boundary and hence the $\ln[\Delta I(x_b)]$ versus x_b plot deviates *upwards* from linearity for small x_b . If $x_b \geq L$ the majority of excess carriers undergo recombination in the bulk before reaching the grain boundary and hence the deviation from linearity in a $\ln[\Delta I(x_b)]$ versus x_b plot will be small. Alternatively there could be a decrease in τ_{r} at the grain boundary due to segregated impurity atoms/vacancies, etc., which give rise to shallow donor/acceptor states. If the decrease in τ_{r} offsets the decrease in τ_{nr} such that overall η increases, the CL emission is increased for a given carrier density at the grain boundary and hence the $\ln[\Delta I(x_b)]$ versus x_b plot deviates *downwards* from linearity for small x_b . This is what is observed in Fig. 1(d) (note that the downward shift could also be due to excess carriers being present on both sides of the grain boundary for small x_b , an effect that was ignored in Eq. (1)). In Fig. 1(d) a straight line was least-squares fitted ignoring the first three data points closest to the grain boundary.

Table I lists the L and S values extracted from the $\ln[\Delta I(x_b)]$ versus x_b plots for three separate CdTe grain boundaries [grain boundary 1 is that shown in Fig. 1(b)]. The correlation coefficient (r^2) for the least-squares fit straight line is also tabulated. In all cases the $\ln[\Delta I(x_b)]$ versus x_b plot

TABLE I. L and S values extracted from three separate grain boundaries in CdTe. The r^2 value for least-squares fitting of $\ln[\Delta I(x_b)]$ versus x_b plots is also shown.

Grain boundary	Correlation coefficient (r^2)	Minority carrier diffusion length (L) (μm)	Reduced recombination velocity (S)
1	0.98	0.55 ± 0.03	0.23 ± 0.02
2	0.99	0.45 ± 0.02	0.29 ± 0.02
3	0.99	0.57 ± 0.02	0.33 ± 0.03

curved downwards for small x_b and hence these data points were excluded from least-squares fitting (it must be noted however that least-squares fitting all data points did not appreciably change L and S). r^2 is close to one which suggests a linear relationship between the data points for large x_b . In p-type CdTe the minority carriers are electrons and their measured diffusion length L is in the range 0.4–0.6 μm . The “water drop” method of Wight *et al.*¹³ gave an electron diffusion length in the range 0.7–3.0 μm for metal organic chemical vapor deposited and liquid phase epitaxial CdTe. Toušková *et al.*² used a contactless photovoltage method to measure an electron diffusion length of 0.5 μm for electrodeposited CdTe. L is dependent on the CdTe synthesis method (presumably due to the presence of point defects such as Cd vacancies¹⁴) as well as doping concentration and any impurities. Nevertheless the electron diffusion length extracted in this study is comparable to measurements using other techniques. The reduced recombination velocity is in the range 0.2–0.3 (Table I), which for $\tau \approx 20$ ns (Ref. 13) and $L \approx 0.5$ μm (this study) gives a recombination velocity of 500–750 cm/s. Such low values could be due to the grain boundaries being subgrain boundaries with small misorientations.¹¹ As a comparison Cohen *et al.*¹⁵ have estimated a *surface* recombination velocity of 5×10^5 cm/s for etched, p-type CdTe from time resolved photoluminescence experiments, three orders of magnitude larger than the recombination velocity obtained for grain boundaries using the CL method.

The van Roosbroeck result⁸ assumes uniform generation of excess carriers along a plane parallel to the grain boundary. Figure 2 shows the Monte Carlo simulated generation volume for a 15 kV electron beam in CdTe. Although a linear relationship was observed between $\ln[\Delta I(x_b)]$ and x_b it is clear that the generation volume is not of the form assumed. First consider the depth variation in the generation volume

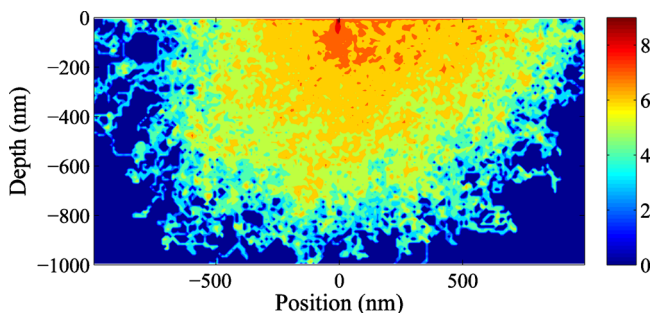


FIG. 2. (Color online) Monte Carlo simulation of electron-hole pair generation by a 15 kV electron beam in CdTe. The number of excess carriers is plotted on a logarithmic scale.

along the beam direction. Electron-hole pairs generated deep within the material are few in number and in general the photons produced by their recombination will be absorbed within the solid [the $1/e$ distance for absorption of the fundamental emission in CdTe is ≈ 0.17 μm (Ref. 16)]. Hence there is a “cut-off” depth for CL detection. Within this cut-off depth generation is at a maximum closer to the beam entrance surface. However, many of these excess carriers are lost to surface recombination, so that the depth variation in the number of carriers is “smoothed out,” giving a better agreement with the van Roosbroeck model. Next consider the lateral width of the generation volume, which broadens the CL profile and leads to a shallower minimum at the grain boundary, with the net result that S is underestimated and L overestimated. A lower beam energy reduces the effects of broadening, although the smaller beam penetration depth means that the entrance surface could significantly modify the steady state carrier distribution from the van Roosbroeck model. An intermediate beam energy is therefore likely to give the most reliable results. More detailed simulations, taking into account surface recombination, are required to determine beam voltages at which the steady state carrier distribution deviates appreciably from the van Roosbroeck model.

In summary, we have developed a contactless method for extracting the reduced recombination velocity and minority carrier diffusion length from the CL intensity profile across an end-on grain boundary. A bulk electron diffusion length of 0.4–0.6 μm and reduced recombination velocity of 0.2–0.3 was obtained for grain boundaries in vapor deposited p-type CdTe. The technique can be used to investigate the effect of grain boundaries on solar cell performance.

B.G.M. would like to thank the Faculty of Science, Durham University and Q.Z.J., the EPSRC (Grant No. EP/D048737/1) for financial support. The authors would also like to thank Mr. Robert Treharne for measuring the CdTe film thickness using a profilometer.

¹A. Shah, P. Torres, R. Tscharnner, N. Wyrsh, and H. Keppner, *Science* **285**, 692 (1999).

²J. Toušková, D. Kindl, and J. Toušek, *Thin Solid Films* **293**, 272 (1997).

³K. Durose, P. R. Edwards, and D. P. Halliday, *J. Cryst. Growth* **197**, 733 (1999).

⁴J. Nelson, *The Physics of Solar Cells* (Imperial College Press, London, 2003).

⁵P. T. Landsberg, *Recombination in Semiconductors* (Cambridge University Press, Cambridge, 1991).

⁶B. G. Yacobi and D. B. Holt, *Cathodoluminescence Microscopy of Inorganic Solids* (Plenum, New York, 1990).

⁷C. M. Parish and P. E. Russell, *Adv. Imaging Electron Phys.* **147**, 1 (2007).

⁸W. Van Roosbroeck, *J. Appl. Phys.* **26**, 380 (1955).

⁹C. Donolato, *J. Appl. Phys.* **54**, 1314 (1983).

¹⁰Q. Jiang, D. P. Halliday, B. K. Tanner, A. W. Brinkman, B. J. Cantwell, J. T. Mullins, and A. Basu, *J. Phys. D: Appl. Phys.* **42**, 012004 (2009).

¹¹C. C. R. Watson and K. Durose, *J. Cryst. Growth* **126**, 325 (1993).

¹²J. I. Goldstein, D. E. Newbury, D. C. Joy, C. E. Lyman, P. Echlin, E. Lifshin, L. Sawyer, and J. R. Michael, *Scanning Electron Microscopy and X-ray Microanalysis* (Springer, New York, 2003).

¹³D. R. Wight, D. Bradley, G. Williams, M. Astles, S. J. C. Irvine, and C. A. Jones, *J. Cryst. Growth* **59**, 323 (1982).

¹⁴A. Castaldini, A. Cavallini, B. Fraboni, P. Fernandez, and J. Piqueras, *J. Appl. Phys.* **83**, 2121 (1998).

¹⁵R. Cohen, V. Lyahovitskaya, E. Poles, A. Liu, and Y. Rosenwaks, *Appl. Phys. Lett.* **73**, 1400 (1998).

¹⁶T. H. Myers, S. W. Edwards, and J. F. Schetzina, *J. Appl. Phys.* **52**, 4231 (1981).